Bioresource Technology 427 (2025) 132389

Contents lists available at ScienceDirect

Bioresource Technology

journal homepage: www.elsevier.com/locate/biortech

Viral RNA reduction from wastewaters using microalgae-based treatments: Elucidating the effect of light and zero-valent iron nanoparticles

Andrés F. Torres-Franco [a,b,*], Deborah Leroy-Freitas [a,b], Pedro A. García-Encina [a,b], Raúl Muñoz [a,b,*]

[a] Institute of Sustainable Processes, Dr. Mergelina, s/n, 47011 Valladolid, Spain
[b] Department of Chemical Engineering and Environmental Technology, School of Industrial Engineering, University of Valladolid, Dr. Mergelina, s/n, 47011 Valladolid, Spain

HIGHLIGHTS

- Microalgae-based reduction of viral RNA of at least 99 % was achieved within 192 h.
- ZVI NPs at high-light intensity supported at least 99 % reduction within 72 h.
- Viral RNA reduction was associated with O_2 and light excess conditions.
- ZVI NPs enhanced MS2/Phi6 reduction by boosting algal-bacterial photo-oxygenation.
- BCoV RNA was inactivated mainly by light-driven mechanisms.

GRAPHICAL ABSTRACT

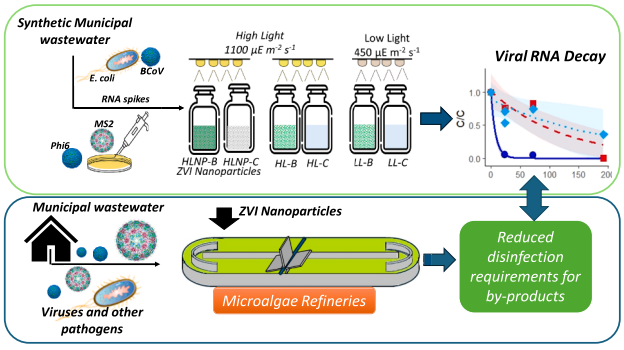

ARTICLE INFO

Keywords:
E. coli
Microalgae-based wastewater treatment
Viral RNA reduction
Zero-valent iron nanoparticles

ABSTRACT

Microalgae-based systems can potentially inactivate *E. coli* and viruses. In this work, batch algal-bacterial photobioreactors were operated to elucidate the effect of zero-valent iron (ZVI) nanoparticles and light intensity on the reduction of viral RNA (MS2, Phi6 and Bovine coronavirus, BCoV) and *uidA* gene (*E. coli*) during secondary wastewater treatment. Biodegradation and abiotic control photoreactors were operated at high light intensity (1100 µE m^{-2} s^{-1}), with and without ZVI-nanoparticles addition (*HLNP* and *HL*) and low light intensity (450 µE m^{-2} s^{-1}), without nanoparticles (*LL*). After 72 h, *HLNP* matched or increased the reductions of at least 99.9 % for viruses and 99 % for *uidA* achieved within 192 h in *HL* and *LL*. Oxidative reactions in the presence of ZVI-nanoparticles seemed to mediate the decay of viral RNA and *uidA*. This work demonstrated for the first time the potential for enhanced reduction of viral RNA and *E. coli* by ZVI-nanoparticles during microalgae-based wastewater treatment.

* Corresponding authors at: Institute of Sustainable Processes, Dr. Mergelina, s/n, 47011 Valladolid, Spain.
E-mail addresses: andresfelipe.torres@uva.es (A.F. Torres-Franco), deborah.leroy@uva.es (D. Leroy-Freitas), pedroantonio.garcia@uva.es (P.A. García-Encina), raul.munoz.torre@uva.es (R. Muñoz).

https://doi.org/10.1016/j.biortech.2025.132389
Received 10 December 2024; Received in revised form 23 February 2025; Accepted 10 March 2025
Available online 13 March 2025

1. Introduction

Microalgal technologies have emerged as promising wastewater treatment systems and biorefinery platforms capable of converting contaminated effluents into value-added by-products, such as pigments, proteins and fertilisers. The key limitation for expanding the market of wastewater treatment-based by-products is their sanitary quality. In this context, many viruses excreted in human and animal faeces are present in municipal and agricultural wastewaters, mediating the transmission of several waterborne diseases such as diarrhoea and hepatitis (McCall et al., 2020). While the complete elimination of viruses from treated effluents and biomass requires disinfection processes, enhancing the reduction of viruses during secondary treatment will significantly minimise the complexity of further disinfection steps.

Recent works have suggested that microalgae-based systems can substantially reduce virus load during secondary wastewater treatment compared to activated sludge or anaerobic reactors (Torres-Franco et al., 2024). The advantage of this solar power technology, which can provide inactivation levels of *E. coli* and other pathogenic bacteria and viruses of up to 99 %, relies on their relatively high hydraulic retention times (HRTs) of 5–8 days for sewage treatment (Young et al., 2016; Ruas et al., 2020; Espinosa et al., 2022; Chambonniere et al., 2023). Further lab-scale experiments suggested the inactivation below detection levels of Phi6 and MS2 viral surrogates within 72 h and 96 h in the soluble fraction of microalgal-bacterial reactors at high light intensities (Torres-Franco et al., 2024). Similarly, a drastic inactivation of MS2 after 8 h by *Nannochloropsis salina* in salt medium (Unnithan et al., 2014) and a high inactivation of somatic coliphages and F-specific coliphages, Enterovirus, and Norovirus GI (1.49 ± 0.16) by Galdieria sulphuraria during real municipal wastewater treatment under acidic conditions (Delanka-Pedige et al., 2020).

Surrogates without major biosafety requirements are usually selected to model viral decays. Among them, MS2 and Phi6 bacteriophages have been commonly applied together for studying viruses in wastewater matrixes (e.g. Titcombe Lee et al., 2016; Ye et al., 2016; Yang et al., 2022; Torres-Franco et al., 2024). Similarly, inactivated RNA from bovine coronavirus (BCoV) has been applied for process control in SARS-CoV-2 monitoring studies (Jafferali et al., 2021). MS2 bacteriophage is a non-enveloped virus of the *Leviviridae* family with a diameter of 20–30 nm and an isoelectric point (IEP) of 2.2–3.6 (Dika et al., 2015). Phi6 is an enveloped bacteriophage, member of the *Cystoviridae* family, with a size of 85 nm and an IEP of <7 (Yang et al., 2022). On the other hand, BCoV belongs to the *Coronaviridae* family, has a viral envelope, a diameter of 220 nm and IEP of 4.45–4.65 (Kapil et al. 1999; Vlasova and Saif, 2021). Phi6 genome is a double-strain RNA (dsRNA), while MS2 and BCoV have single-strain RNA genomes (ssRNA). The virus partitioning to solids in wastewater may be influenced by IEP, capsid proteins, and virus particle size (Ye et al., 2016; Yang et al., 2022), which, in addition to factors such as the absence of viral envelope or DNA dsRNA genome, may increase their survival in wastewater environments (Decrey et al., 2015; Harrison et al., 2023). In this sense, MS2, Phi6 and BCoV are typically used as surrogates since they represent a wide range of fecal-borne viruses such as coliphages, norovirus or SARS-CoV-2, as demonstrated by their relatively similar decay rate constants (k) in a broad range of about 0.1 to 2.5 d^{-1} (Kennedy et al., 2023; Silverman and Boehm, 2020; Torres-Franco et al., 2024). Finally, since most *E. coli* strains possess the *uidA* gene encoding β-D-glucuronidase (GUS) activity, this gene has been used to proxy the presence and survival of *E. coli* in wastewater treatment plants and river waters (García et al., 2022).

On the other hand, recent advances in microalgae-based systems have shown that some nanoparticles (NPs) can enhance microalgae growth (Vargas-Estrada et al., 2020). Particularly, zero valence iron (ZVI) NPs enhanced the performance of algal-bacterial photoreactors during biogas upgrading (Vargas-Estrada et al., 2023). In addition, several works have assessed the disinfection potential of iron-based NPs in water matrixes (e.g. Gutierrez et al., 2009; Nieto-Juarez & Kohn, 2013), among which ZVI NPs demonstrated a high capacity for E. coli (Wang et al., 2022) and virus inactivation (Kim et al., 2011), likely mediated by the production of extracellular reactive oxygen species (ROS) under aerated conditions. Unfortunately, there is a lack of research on the effect of ZVI NPs on viruses and E. coli during microalgal-based municipal wastewater treatment. Thus, this study assessed the decay of RNA of MS2, Phi6, BCoV, and *uidA* gene from *E. coli* in batch-wise operated algal-bacterial photoreactors, demonstrating, for the first time, the feasibility of ZVI NPs application to facilitate further disinfection steps when higher sanitary quality may be required for effluent or biomass reuse applications.

2. Material and methods

2.1. Synthetic wastewater and microalgae inoculum

Synthetic municipal wastewater (*SMWW*) was used in the experiments to avoid biases from the typical fluctuations of real wastewater composition. *SMWW* was freshly prepared before the experiment, as described in Frutos et al. (2016). A stock solution with the inorganic compounds (10 × concentration) was diluted in distilled water before autoclaving. The organic compounds were added inside the sterile bench at the beginning of the experiment. *SMWW* was characterised by a pH of 7.7 ± 0.1 and concentrations of dissolved total organic carbon (TOC) of 252 ± 11 mg L^{-1}, dissolved inorganic carbon (IC) of 23 ± 3 mg L^{-1}, and 63 ± 2 mg L^{-1} of dissolved total nitrogen (TN).

The algal-bacterial inoculum was obtained from a pilot high rate algal pond treating municipal wastewater in Almeria (Spain). The inoculum was dominated by chlorophytes, had a density of $>10^6$ cell mL^{-1}, and exhibited a pH of 9.46, dissolved oxygen (DO) of 4.35 mg L^{-1} and concentrations of total and volatile suspended solids (TSS and VSS) of 0.59 and 0.58 g L^{-1}, respectively.

2.2. Viral stocks

Active cultures of bacteriophages Phi6 and MS2, along with RNA from inactivated BCoV in the Scourguard® vaccine, were used as viral RNA models and spiked into batch photoreactors in order to assess their reduction over time. Stock solutions of the bacteriophages Phi6 and MS2 were achieved by applying the same procedure described in Torres-Franco et al. (2024) via propagation of an active culture of Phi6 (DSM-21518) and freeze-dried MS2 (DSM-13767) and their respective host, *Pseudomonas* sp. (DSM-21482) and *E. coli* (DSM-55695), all purchased from DSMZ (German Collection of Microorganisms and Cell Cultures). Bacteriophage stock suspensions were tittered using the double agar technique (Fedorenko et al., 2020). High titers of 2.9×10^{11} and 1.2×10^{14} PFU mL^{-1} were quantified in the Phi6 and MS2 stocks, respectively, at the beginning of the experiment. The lyophilised phase of the Scourguard® cattle vaccine, containing *E. coli*, was dissolved in the provided serum before being spiked into the reactors. Viral stocks showed RNA concentrations of 5.6×10^{10}, 2.6×10^{14}, and 1.5×10^{7} genomic copies (gc) L^{-1} for Phi6, MS2 and BCoV, respectively. On the other hand, the *uidA* gene in the MS2 stock solution and Scourguard® vaccine had concentrations of 1.7×10^{10} and 1.0×10^{10} gc L^{-1}. Mengovirus (MgV), a non-enveloped member of the *Picornaviridae* family, was used as a standard for process control (Randazzo et al., 2020). A stock of MgV with 8.2×10^{12} gc L^{-1} was purchased from the CECT (MVo, CECT 10000) and spiked to samples before RNA extraction.

2.3. Zero-valent iron nanoparticles

Low-cost carbon-coated ZVI NPs produced from olive oil residues using hydrothermal carbonisation (HTC) techniques were kindly donated by SMALLOPS NPS (Spain). The ZVI NPs contained 31.38 % (wt %) of iron, a particle size of 150 nm and traces of elements such as P, K, Ca and S (Vargas-Estrada et al., 2023).

2.4. Experimental set-ups

Three operational conditions were batch-wise tested in parallel using 2.1 L sterile glass bottles (Fisher) to assess the potential of microalgae to conduct secondary wastewater treatment and viral RNA reduction. All treatments were carried out in duplicates, comparing biotic and abiotic conditions. In the first biodegradation test series (High light intensity + NPs addition, *HLNP-B*), 500 mL of microalgae were inoculated in 500 mL of *SMWW* and supplemented with ZVI NPs at a concentration of 20 mg L^{-1}, at which growth enhancement and no harmful effects on microalgae were identified (Vargas-Estrada et al., 2023). The bottles were maintained under high light intensity (1100 μE m^{-2} s^{-1}). Test series 2 and 3 were carried out without adding ZVI NPs. In test series 2 (High light intensity, *HL-B*), the same high light intensity was applied in systems prepared as described above, whereas, in test series 3 (Low light intensity, *LL-B*), illumination was provided at low intensity (450 μE m^{-2} s^{-1}). Duplicates of *SMWW* control reactors (*HLNP-C, HL-C*, and *LL-C*) without microalgae inoculation were run under all operational conditions tested to assess the influence of the main abiotic conditions (nanoparticles presence and light intensity).

All experiments were conducted in a temperature-controlled room set at 25 °C. A panel of white LED lamps (Phillips, Spain) illuminated *HLNP* and *HL*, while a second panel connected to a dimmer provided light in *LL*. All reactors were illuminated with a photoperiod of 24 h. Agitation was provided with magnetic stirrers at 180 rpm (Cimarec I Multipoint, Thermofisher).

After inoculating the biodegradation photoreactors at sterile conditions, all bottles were capped with butyl septa, flushed with Helium (>99.9 %, Abello Linde, Spain), and agitated for 20 min to achieve gas–liquid equilibrium. Then, all biodegradation and control photoreactors were spiked with the viral suspensions of active cultures of Phi6 and MS2 and Scourdguard® vaccine at a ratio of 1:1000. Before collecting the initial samples (t = 0 h), an additional incubation time of 15 min was established to allow the complete mixing of the viral suspensions in the liquid phase of the control and biodegradation reactors.

The experiments were conducted for 192 h, with daily sampling of the liquid and gas phases. The headspace of the control and biodegradation reactors was sampled by withdrawing 100 μL with a gas-tight syringe (Hamilton, USA) to monitor O_2, CO_2, H_2S, and CH_4 concentrations by GC-TCD. Liquid samples (20 mL) were collected using syringes (10 mL) with needles (21G, 0.82 mm) directly from the biodegradation and control photoreactors under sterile conditions. Liquid samples were stored in 50 mL falcon tubes after the previous reservation of an aliquot of 2 mL in microtubes for assessing viral RNA. The pH and optical density (668 nm) of the cultivation broths was measured immediately after liquid sample withdrawal. Then, the liquid samples were filtered through 0.22 μm pore-sized membranes to determine the concentrations of TOC and TN. Additional unfiltered aliquots were drawn to determine TSS and VSS at 0 h, 96 h and 192 h.

The partitioning and survival of viral RNA were assessed using the 2 mL aliquots previously stored for this purpose. The fraction of viral RNA in the soluble phase was evaluated by processing 1 mL of the sample through an adaptation of the method described by Espinosa et al. (2021) by centrifuging at 4,000 g for 20 min at 4 °C and separating the supernatant using sterile needles (23G, 0.64 mm) and syringes (2 mL), following filtration through 0.22 μm pore-size membranes (Merck SLGPM33RS). Total and filtered samples were spiked with 20 μL of the MgV (CECT 10000) stock solution and gently vortexed before being stored at −80 °C for further RNA extraction.

2.5. Physical-chemical analytical procedures

Gas concentrations were analysed in a Gas Chromatograph (8860 GC-TCD System, Agilent, USA) equipped with a thermal conductivity detector. A benchtop pH BASIC20 (Crison, Spain) was used for pH. Optical density was measured in a BMG UV/vis spectrometer. Concentrations of TOC and TN were measured from filtered samples using a TOC-VCSH TOC analyser equipped with a TMN-1 unit (Shimadzu, Japan). TSS and VSS concentrations were determined according to Standard Methods for Water Examination (Rice et al., 2012).

2.6. RNA extraction, RT-qPCR and recovery assessment

Samples withdrawn at 0 h, 24 h, 72 h, and 192 h were selected for tracking viral decays. For this purpose, viral RNA was extracted directly from 200 μL sample aliquots (without viral concentration step) using the AllPrep PowerViral DNA/RNA Kit (Qiagen), according to the manufacturer's instructions. The RNA was eluted in 100 μL of the provided buffer, and the resulting RNA concentrations were measured using a Qubit 4 (Thermofisher) with Qubit RNA high-sensitivity (HS) assay kits. The RNA was stored at −80 °C until further analysis.

Quantifications for the assessment of survival (Phi6, MS2, BCoV), uidA gene from *E. coli* and recovery control (MgV) of viral RNA in filtered and total samples were performed using reverse-transcription quantitative real-time PCR (RT-qPCR) in a QuantStudio 1 (Applied Biosystems, USA), using 96-well plates. All RT-qPCR reactions for viral RNA quantification were designed using a TaqPath 1-Step RT-qPCR Master Mix (Applied Biosystems, USA), with a total volume of reaction of 20 μL, containing 5 μL of Master Mix and 5 μL of RNA template. Primers and probes, including concentrations and sequences, are described in Table 1. All RT-qPCR assays were performed following the same cycling conditions: reverse transcriptase at 45 °C for 10 min; polymerase activation at 95 °C for 10 min; 40 cycles of denaturation at 95 °C for 15 s and annealing/extension at 60 °C for 45 s. For gene copy number quantification, standard curves for each strain were built based on serial dilutions of commercial standards (MS2: Roche Applied Sciences, MgV: CECT 10000) and synthetic sequences ordered as a "gBlock" TM gene fragment (IDT, USA). Synthesised gBlocks followed Genebank accessions DQ785287 (2602 bp), M27474.1 (126 bp) and AY698409.1 (647 bp) for Phi6, BCoV and uidA, respectively.

The QuantStudio Design and Analysis Desktop Software was used to analyse the results. All standard curves showed R^2 values above 0.99, and amplification efficiencies between 90 % and 110 %. The threshold, standard curve efficiencies and slopes (m) are presented in the Supplementary Material. The limit of detection of each assay (ALoD) was calculated as in Verbyla et al. (2016) and corresponded to the number of copies per reaction with a 95 % probability of amplification. The ALOD was determined in each case by fitting the exponential survival $P_a(x) = 1 - e^{-dx}$ (using nonlinear regression in Solver −Excel®). In this equation, x represents the mean number of target genome copies added to each qPCR well (mean concentration per reaction), and d represents the probability of "survival". The ALoD estimated in gene copies per reaction (gc r_x^{-1}) for MS2, Phi6, BCoV and *uidA* were 0.46 gc r_x^{-1}, 0.07 gc r_x^{-1}, 0.01 gc r_x^{-1} and 0.01 gc r_x^{-1}, respectively. All samples (total and filtered) achieved recovery efficiencies above 1 %, validating the extraction and quantification steps (see Supplementary Material).

2.7. Data treatment and statistical analyses

TOC and TN removal from the liquid phase, and the overall microalgae biomass productivity, were calculated based on initial and final concentrations of TOC, TN, and VSS. Cycle threshold (Cq) values obtained for Phi6, MS2, BCoV, and *uidA* at 24 h, 72 h and 192 h (Cq_t) were used to estimate the experimental survival of viral RNA detected at time 0 h (Cq_0) (Eq. (1). Similarly, the recoveries of MgV were estimated using the difference between the Cq values quantified in each sample and the Cq of the undiluted MgV (ΔCq_{MV}) referenced by the slope of the standard curve of the RNA of this control virus (Eq. (2) (ISO 15216-1, 2017). The reductions ($\log_{10}$ units) were estimated based on gene copies detected in the photoreactors at 24 h, 72 h and 192 h (gc_t) and the initial copies (gc_0) in the photoreactors (Eq. (3) for each virus, according to

Table 1
List of primers and probes used for RT-qPCR reactions.

Virus	Primer (5́ –> 3́)	Concentration (nM)	Sequence	References
Phi6	Forward	300	CGTACAACCGAGTAGGTTCGT	Miranda & Steward (2017); Kim et al. (2021)
	Reverse	300	GTTAGGCGTCGGGACCATC	
	Probe	250	TCATCCTGCAAGCGTCGCCAATTAAGGC	
MS2	Forward	300	GTCCATACCTTAGATGCGTTAGC	Kingsley et al. (2017); Miranda & Steward (2017)
	Reverse	300	CCGTTAGCGAAGTTGCTTGG	
	Probe	250	ACGTCGCCAGTTCCGCCATTGTCG	
BCoV	Forward	600	CTGGAAGTTGGTGGAGTT	Decaro et al. (2008); Greenwald et al. (2021)
	Reverse	600	ATTATCGGCCTAACATACATC	
	Probe	250	CCTTCATATCTATACACATCAAGTTGT T	
MgV	Forward	500	GCGGGTCCTGCCGAAAGT	Coudray-Meunier et al. (2016); UNE-EN ISO 15216-1
	Reverse	900	GAAGTAACATATAGACAGACGCACAC	
	Probe	250	ATCACATTACTGGCCGAAGC	
uidA	Forward	400	GTGTGATATCTACCCGCTTCGC	Chern et al (2009); García et al. (2022)
	Reverse	400	AGAACGGTTTGTGGTTAATCAGGA	
	Probe	100	TCGGCATCCGGTCAGTGGCAGT	

* All Taqman probes were labeled with 6-carboxyfluorescein (FAM) and with Black Hole Quencher 1 (BHQ-1) at the 5′ and 3′ ends.

their standard curves. Partitioning to solids (Eq. (4) was calculated for the same sampling times.

$$\frac{Cq_t}{Cq_0} = 10^{\frac{Cq_0 - Cq_t}{m}} \quad (1)$$

$$\text{MgV Recovery}\ (\%) = 10^{\frac{\Delta Cq_{MgV}}{m_{MgV}}} \quad (2)$$

$$Log_{10}reduction = log_{10}\left(\frac{gc_o}{gc_t}\right) \quad (3)$$

$$Solidspartitioning(\%) = 1 - 10^{\left(\frac{Cq(total) - Cq(soluble)}{m}\right)} \quad (4)$$

In addition, the experimental decay observed for viral RNA of Phi6, MS2 and BCoV, and *uidA*, over time ($\frac{Cq_t}{Cq_0}$) was fitted to linear and non-linear models (Torres-Franco et al., 2024) using the self-starting functions for analysis of Dose-Response Curves in the *drc* and *aomisc* packages in Rstudio (Ritz et al., 2015; Onofri, 2020). The best model was selected in terms of the lower root-mean-square errors (RMSE) and significant decay rates ($p < 0.05$). In most cases, the best model was the exponential function (Eq. (5) solved using the *DRC.expodecay*() function. However, the same function presented better RMSE when parametrised as Eq. (6) in other cases.

$$\frac{Cq_t}{Cq_0} = ae^{-kt} \quad (5)$$

$$\frac{Cq_t}{Cq_0} = de^{-\frac{t}{e}} \quad (6)$$

In Eq. (5) k is the constant relative exponential decay rate (log_{10}), and a is the value of $\frac{Cq_t}{Cq_0}$ measured at time 0 h (close to 1), following the conventional parametrization in the Chick's model. In Eq. (6), d is equivalent to a, and e corresponds to $1/k$. The *ggplot2* package was used to plot the model fitted to each treatment. The decay comparison was based on T_{90} (the time to achieve a 90 % reduction from the initial Cq) and was determined by solving the equations of the best-fitting model. The minimum and maximum T_{90} estimated for each decay corresponded to the minimum and maximum limits obtained from the standard error of each model fit. A Kruskall-Wallis H-test followed by a Dunn's post-hoc was applied to assess significant differences in T_{90} values between biodegradation photoreactors.

3. Results

3.1. Wastewater treatment performance

Microalgal-bacterial activity was confirmed in all test series through the increases over time in pH, headspace O_2, optical density (O.D), and removal of TN and TOC (Fig. 1). Intense microalgal activity in *HLNP-B* resulted in rapid pH, headspace O_2 and O.D increases, with pH and O_2 above 9.0 and 40 % (v/v) and maximum O.D achieved within the first 48 h (Fig. 1a, 1d, 1 g). Similarly, TN and TOC removal efficiencies of 52 % and 70 % were achieved in *HLNP-B* within the first 24 h (Fig. 1j, 1 m). The maximum TN removal of 70 % in this treatment coincided at 96 h with higher biomass productivities of 0.06 ± 0.00 gVSS L^{-1} d^{-1} compared to 0.03 ± 0.00 gVSS L^{-1} d^{-1} after 192 h.

In *HL-B* and *LL-B,* consistent pH, headspace O_2, and O.D increases occurred only after 120 h and 196 h, respectively (Fig. 1), indicating a less intense microalgal activity than in *HLNP-B,* at least during the first 72 h of batch treatment. High TN and TOC removals of up to 60 % and 78 % were achieved at 96 h in *HL-B* and 71 % and 82 % after 120 h in *LL-B* (Fig. 1k, 1l, 1n, 1o). Biomass productivities at 96 h were 0.05 ± 0.01 gVSS L^{-1} d^{-1} and 0.06 ± 0.01 gVSS L^{-1} d^{-1} in *HL-B* and *LL-B* and final productivities of 0.03 ± 0.0 gVSS L^{-1} d^{-1} were recorded in both biodegradation photoreactors.

3.2. Reduction of viral RNA and uidA fingerprint in algal-bacterial photoreactors

Maximum reductions of MS2 of at least 5.1 log_{10} units were achieved in the bulk fraction of both *HLNP-B* and *HL-B* within 72 h and 192 h, respectively (Fig. 2a, 2e). An increase in MS2 RNA detected at 192 h in the bulk fraction decreased the reductions in *HLNP-B* achieved at 72 h. A lower share of at least 3.9 log_{10} units was achieved in *LL-B* after 192 h (Fig. 2i). Similarly, maximum reductions in the soluble fractions were achieved at 72 h in *HLNP-B* and 192 h in *HL-B* and *LL-B* at 192 h, with 5.7, 5.9, and 4.1 log_{10} units, respectively.

For Phi6, BCoV, and *uidA*, all biodegradation reactors showed relatively similar reduction capacities (Fig. 2). For Phi6, *HLNP-B* achieved the highest reductions after 72 h in the bulk and soluble fractions, with at least 3.7 and 3.5 log_{10} units, respectively (Fig. 2b). Similar to MS2, a slight increase in the concentration of Phi6 in the soluble fraction of *HLNP-B* occurred between 72 h and 196 h. In *HL-B* and *LL-B*, maximum Phi6 reductions were achieved at 196 h, with 2.9 and 2.8 log_{10} units in the bulk fraction and 2.7 and 2.8 log_{10} units in the soluble fractions of each photoreactor, respectively. A different behaviour was observed for BCoV, where *HLNP-B* reduced at least 4.0 log_{10} units only at 192 h (Fig. 2c). Lower BCoV reductions than in *HLNP-B* of 3.8 and 3.7 log_{10} units were achieved in the bulk fraction *HL-B* and *LL-B* at 192 h. In the

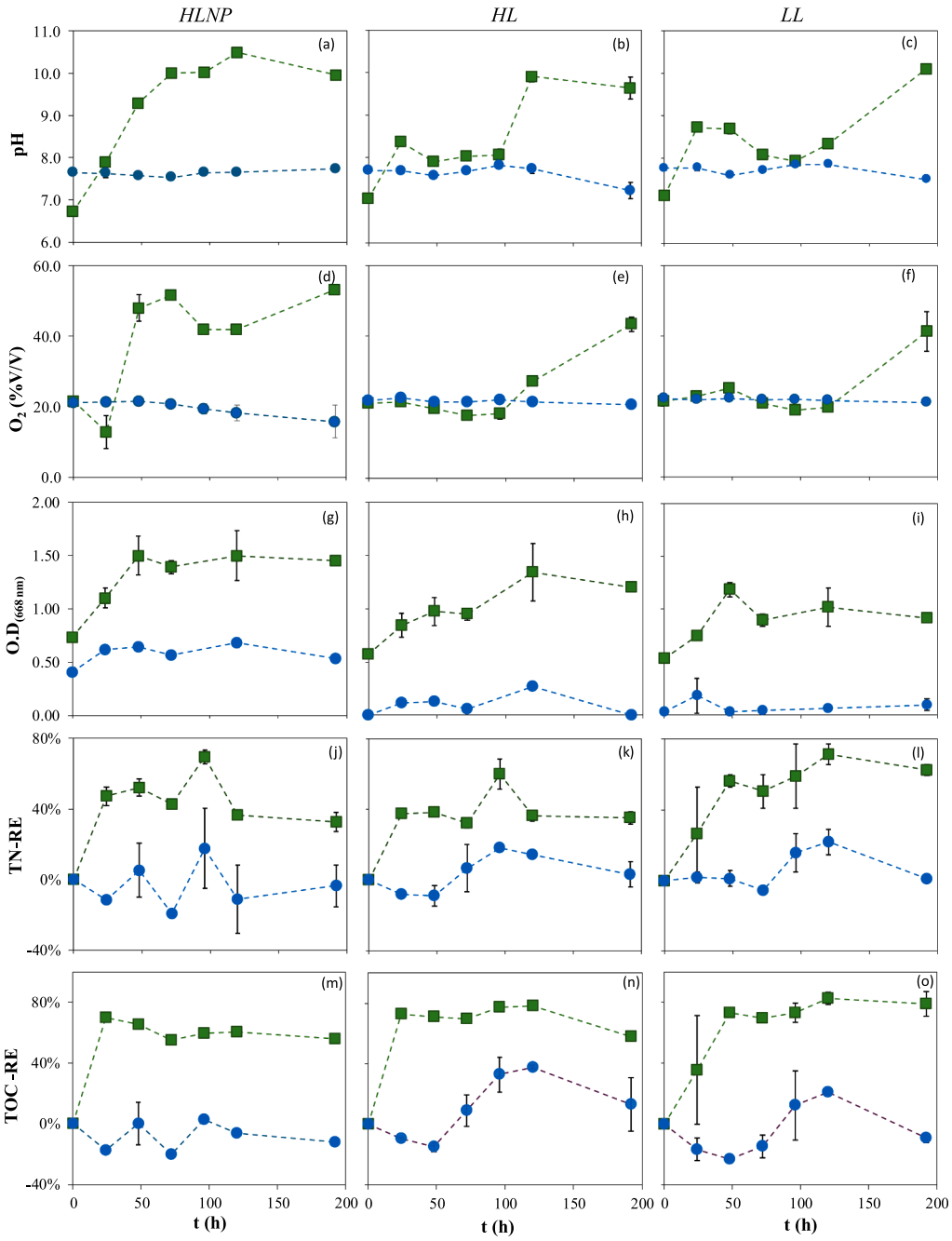

Fig. 1. Average pH, headspace O_2 (%V/V), Optical density (OD) at 668 nm, Total nitrogen (TN-RE) and Total Organic carbon removal efficiencies (TOC-RE) in (a, d, g, j, m) *HLNP*, (b, e, h, k, n) *HL* and (c, f, i, l, o) *LL*'s (■) biodegradation and (●) control photobioreactors (Error bars represent standard deviation-SD. Visible SD bars corresponded to values starting at 0.3 pH units, 2 % (V/V) for headspace O_2 and 7 % TN and TOC-RE).

soluble fractions, only 1.3 and 1.4 $\log_{10}$ units were respectively reduced. Regarding the *uidA* gene, the highest reductions were achieved in *HLNP-B* after 192 h, with at least 2.5 and 2.4 $\log_{10}$ units in the bulk and soluble fraction (Fig. 2d). These shares were higher than reductions of at least 1.9 and 2.1 $\log_{10}$ units achieved in the bulk fraction of *HL-B* and *LL-B,* with very similar values in the soluble phase (Fig. 2h and l).

In terms of efficiencies, *HLNP-B* showed the highest reductions in the bulk fraction for MS2 (99.9999 %) and *uidA* (99.7 %) within 72 h and 192 h, respectively (Table 2). In the case of Phi6 and BCoV, the performance of *HLNP-B* at 72 h (99.9 %) matched that of *HL-B* and *LL-B,* achieved only after 192 h. Additionally, *HLNP-B* showed the highest BCoV (98.2 %) and *uidA* RNA reductions in the soluble fraction.

3.3. Reduction of viral RNA and uidA fingerprint in abiotic photoreactors

No O_2 headspace pH or D.O increases were observed in the control photoreactors under abiotic conditions (Fig. 1). Low MS2's RNA reductions of about 0.7, 0.4 and 0.1 $\log_{10}$ units were achieved in *HLNP-C*, *HL-C* and *LL-C,* respectively (Fig. 2a, 2e and 2i). Similarly, the reductions of Phi6 in the control photoreactors accounted for about 0.5, 1.7, and 1.1 $\log_{10}$ units, respectively (Fig. 2b, 2f and 2i). Considerable higher reductions of 3.0, 4.0 and 3.2 $\log_{10}$ units were recorded in the abiotic reactors for BCoV (Fig. 2c, 2 g and 2 k). In the case of *uidA*, only a marginal removal of 0.4 $\log_{10}$ units occurred in *HLNP-C* (Fig. 2d). In contrast, this gene increased its copy numbers in *HL-C* and *LL-C*. All abiotic photoreactors achieved lower efficiencies than their algal-

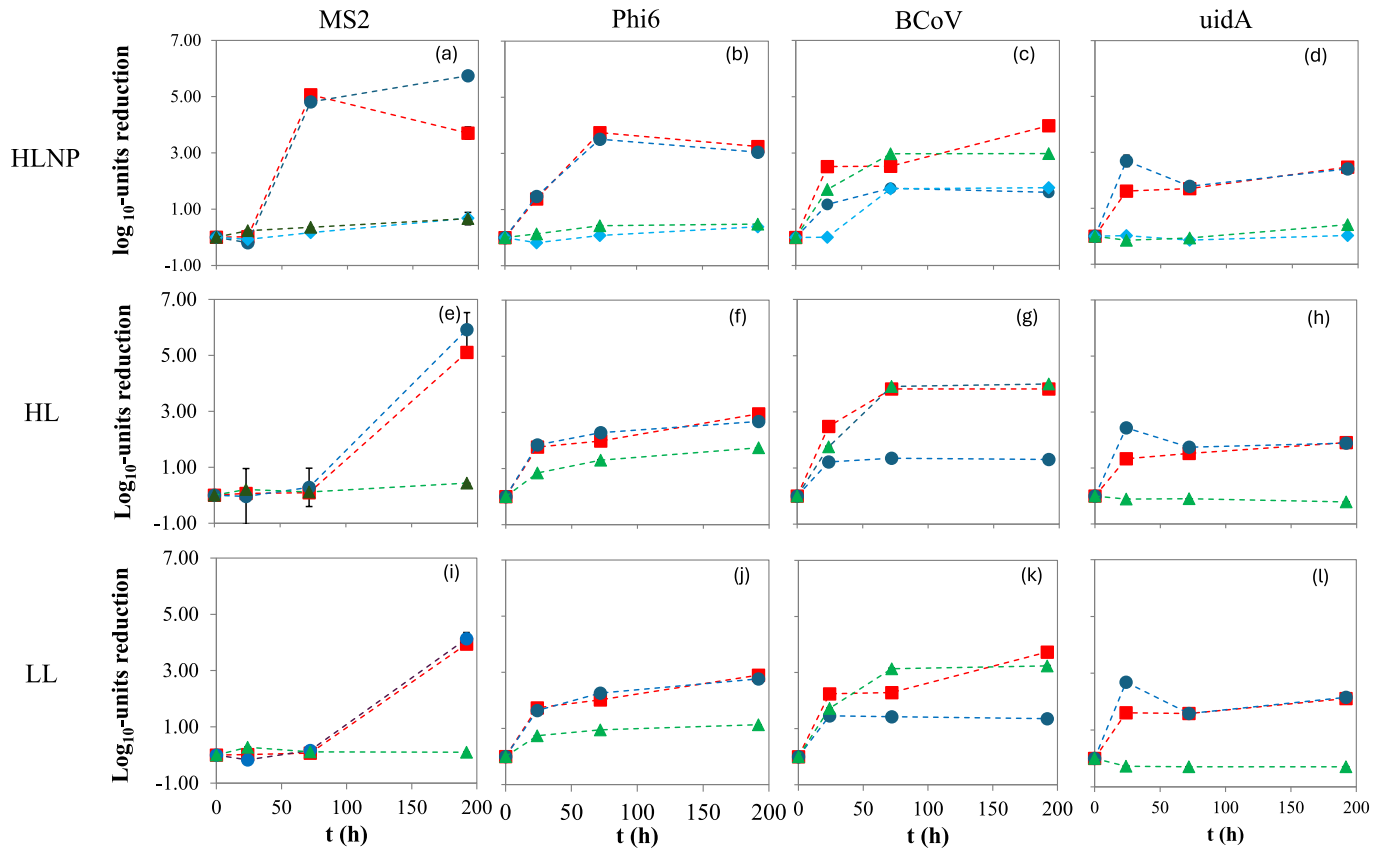

Fig. 2. Average log_{10}-units reduction of RNA from MS2, Phi6, BCoV and *uidA* gene in (■) bulk and (●) soluble fractions of biodegradation photoreactors in (a, b, c, d) *HLNP*, (e, f, g, h) *HL* and (i, j, k, l) *LL*, including (▲) bulk and (♦) soluble fractions of abiotic controls (Error bars represent standard deviation −SD. Visible SD corresponded to values starting at 0.6 log_{10}-units).

Table 2
Maximum removal efficiencies achieved in the algal-bacterial biodegradation (*B*) and control (*C*) photoreactors and in total (T) and soluble (S) fractions (Treatments: High light intensity + zero-valent iron nanoparticles, *HLNP*; High light intensity, *HL*; Low Light intensity, *LL*).

Treatment		Maximum removal efficiencies			
		MS2	Phi6	BCoV	*uidA*
HLNP	*B*	T: 99.9999 % (72 h) S: 99.999 % (72 h)	T: 99.9 % (72 h) S: 99.9 % (72 h)	T: 99.99 % (192 h) S: 98.2 % (72 h)	T: 99.7 % (192 h) S: 99.6 % (192 h)
	C	T: 78 % (192 h) S: 79 % (192 h)	T: 66 % (192 h) S: 59 % (192 h)	T: 99.9 % (192 h) S: 98.3 % (192 h)	T: 61.8 % (192 h) S: 6.5 % (192 h)
HL	*B*	T: 99.999 % (192 h) S: 99.9999 % (192 h)	T: 99.9 % (192 h) S: 99 % (192 h)	T: 99.98 % (192 h) S: 95.5 % (72 h)	T: 98.7 % (192 h) S: 98.7 % (192 h)
	C	63 % (192 h)	98 % (192 h)	99.99 % (192 h)	S: Growth
LL	*B*	T: 99.99 % (192 h) S: 99.99 % (192 h)	T: 99.9 % (192 h) S: 99.8 % (192 h)	T: 99.98 % (192 h) S: 96.5 % (24 h)	T: 99.2 % (192 h) S: 99.3 % (192 h)
	C	50 % (192 h)	93 % (192 h)	99.9 % (192 h)	Growth

bacterial counterparts (Table 1), except for the removals of BCoV in the soluble fraction of *HLNP-B* and *LL-B*.

3.4. Decay kinetics

The RNA fingerprint decay kinetics were assessed for all target genes. Fig. 3 shows the best model fit for each virus in algal-bacterial and control photoreactors. First-order exponential decay resulted in significant parameters and lower RMSE values (Supplementary Material). The decay rates and T_{90} values calculated from these models are presented in Table 3. The higher reductions achieved in the algal-bacterial photoreactors compared to the abiotic photoreactors were confirmed by the higher *k* rates and significantly lower T_{90} values recorded in the algal-bacterial photoreactors. MS2 *k* rates ranged from −0.008 to −0.021 h^{-1} in the bulk fraction of algal-bacterial photoreactors, showing consistently lower values than Phi6, BCoV and *uidA*, with *k* rates ranging from −0.1 to −0.2 h^{-1}. A similar trend was observed for T_{90}, with calculated values of more than 115 h for MS2 and less than 48 h in all algal-bacterial photoreactors for the other target genes. In the abiotic controls, T_{90} values of more than 192 h were calculated for MS2's RNA, whereas Phi6 and BCoV showed T_{90} of less than 48 h.

Pairwise comparisons of T_{90} values revealed further improvements in the algal-bacterial photobioreactors, mainly in the decay of MS2's RNA, for which more relevant differences were detected among treatments. For this bacteriophage, the T_{90} measured in the bulk fraction of *HLNP-B* was the lowest achieved compared to the same level of reduction in *HL-B* and *LL-B*. Nonetheless, *HL-B* fostered the fastest decay of MS2 in the soluble fractions, with a T_{90} of 18.7 h. For Phi6 and BCoV, low T_{90} values in the bulk and soluble fractions were achieved in *HL-B* and *LL-B*, showing short differences compared with *HLNP-B*, which achieved rapid removals within 24 h of at least 90 % of these genes RNA.

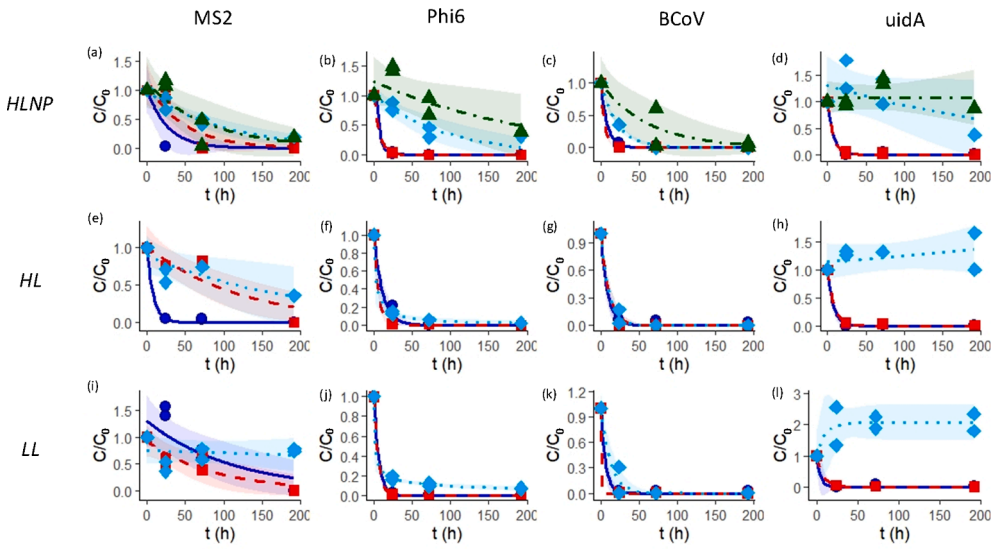

Fig. 3. Decay curves calculated for RNA from MS2, Phi6, BCoV, and *uidA* gene in the (■) total and (●) soluble fractions in the algal-bacterial and (♦) control photobioreactors of (a, b, c, d, e) *HLNP*, (e, f, g, h) *HL* and (i, j, k, l) *LL* treatments. In *HLNP* abiotic control, the decay in the (▲) total fraction was also assessed. Each marker represents an experimental duplicate. Ribbons correspond to the standard error of each regression.

In addition, while abiotic controls showed increases over time of *uidA* gene, all algal-bacterial photoreactors resulted in decays of this marker, with relatively similar *k* rates and no significant differences in T_{90} among treatments, neither in the total nor the soluble fractions.

4. Discussion

Photosynthetic activity was confirmed by pH and DO increases in all algal-bacterial photoreactors and resulted in all treatments in TN and TOC removals within typical ranges for microalgae-based municipal wastewater treatments above 50 % and 60 %, respectively (Espinosa et al., 2021; Posadas et al., 2015; Ruas et al., 2020). The addition of ZVI NPs in *HLNP-B* induced within 24 h to 96 h a faster photo-oxygenation and high TN and TOC removals compared to *HL-B* and *LL-B*, which achieved high treatment efficiencies only after 96 h and 120 h, respectively. ZVI NPs boosted microalgal growth likely by providing extra Fe and stimulating nutrients uptake on the microalgal surfaces (Vargas-Estrada et al., 2023; Wang et al., 2024). Nevertheless, biomass productivities in *HLNP-B* were lower than those reported by Vargas-Estrada et al. (2023), with 0.5 g L^{-1} d^{-1} after 96 h of batch growth. Since no toxic effect or decrease in lipid and carbohydrate content in microalgae biomass were observed when SMALLOPS NPs were used in microalgae at the low dosage of 20 mg L^{-1} (Vargas-Estrada et al., 2023), the low productivities could be explained by the low loads of carbon and nutrients in *SMWW* driving an endogenous metabolism after prolonged photo-aeration beyond 96 h. Similarly, the exhaustion of nutrients after 120 h could have caused the relatively low productivity in *HL-B*. Conversely, the slower growth of microalgae and less intense nutrient uptake in *LL-B* explains its higher productivities, which were comparable to those of up to 1 g L^{-1} d^{-1} achieved in batch photobioreactors operated at similar HRT of 196 h and light intensities (Gonzalez-Camejo et al., 2019).

4.1. Viral RNA and uidA reduction in algal-bacterial photoreactors

Previous works assessing viral decay in secondary wastewater treatment technologies suggested an association between the inactivation of viruses and high carbon and nutrient treatment efficiency (Prado et al., 2018). Indeed, all algal-bacterial photoreactors supported a high performance in viral RNA and *E. coli-uidA* gene reduction, achieving at least a 99 % removal in the bulk fraction by 192 h of batch treatment. Viral RNA reduction was associated with pH increases, headspace O_2 accumulation and TN and TOC removal in all biodegradation photoreactors, particularly for MS2 bacteriophage. Maximum MS2 reductions, achieved at 72 h in *HLNP-B* and 192 h in *HL-B* and *LL-B,* broadly coincided with high TOC and TN removals, achieved at less than 96 h in *HLNP-B* but at longer periods in *HL-B* and *LL-B*. The slight increase in MS2 RNA detected at 192 h could result from MS2 replication in the presence of a bacterial host, likely due to the adaptation of some viral subpopulations to the environmental conditions in *HLNP-B*. Nonetheless, the decay parameters confirmed the faster MS2 decay in the bulk fraction of *HLNP-B* compared to the other biodegradation photoreactors.

The reduction of MS2 fingerprint in all photoreactors was probably associated with highly oxidative conditions mediated by photo-oxygenation, as evidenced by the association between RNA reduction and increases in O_2 concentrations. In *HLNP-B*, the presence of ZVI NPs contributed indirectly to viral and *uidA* RNA decay by enhancing algal metabolism and photo-oxygenation. ZVI NPs could also contribute to MS2 and other viral RNA removal by disrupting virions at contact (Kim et al., 2011; Kim et al., 2021). Overall, the presence of ZVI NPs at high light intensities enhanced the performance in *HLNP-B* by reducing the time required to achieve higher treatment efficiencies and high viral and *uidA* RNA reductions from the bulk fraction compared to *HL-B* and *LL-B*. Nevertheless, the performance of NPs seemed to be higher within 96 h of batch treatment. Higher retention times may lead to endogenous metabolisms and lower treatment efficiencies and RNA reductions, especially during the treatment of low carbon and nutrients concentrations in municipal wastewater.

Phi6 and BCoV's lower T_{90} compared to MS2 confirmed previous observations in which enveloped viruses were less resistant than non-enveloped (Ye et al., 2016; Yang et al., 2022) during wastewater treatment. Besides their lower resistance, Phi6 and BCoV also showed higher initial partitioning and higher affinity to solids than MS2 in all algal-bacterial photoreactors (see Table 4). In the case of BCoV, relatively similar decay parameters and overall reductions achieved in the soluble fractions of the algal-bacterial and control photoreactors suggest that photoinactivation was likely the primary mechanism for RNA removal. This mechanism also seemed to explain the higher decay rates achieved in the soluble fraction of *LL-B*. Microalgal growth was slower in this photoreactor, resulting in lower TSS concentrations during the first 24 h and allowing a higher light penetration than in *HLNP-B* and *HL-B*. In these treatments, the presence of NPs and the growth of microalgal

Table 3
Decay parameters (log_{10}-k rates and T_{90}) for MS2, Phi6, BCoV and *uidA* RNA reduction in algal-bacterial biodegradation (*B*) and control (*C*) photoreactors and in total (T) and soluble (S) fractions (Treatments: High light intensity + zero-valent iron nanoparticles, *HLNP*; High light intensity, *HL*; Low Light intensity, *LL*).

Treatment		log_{10}-k rates (h^{-1})				T_{90} (h)			
		MS2	Phi6	BCoV	*uidA*	MS2	Phi6	BCoV	*uidA*
HLNP	*B*	T: −0.021 ± 0.07 S: −0.037 ± 0.07	T: −0.134 ± 0.003 S: −0.142 ± 0.004	T: −0.192 ± 0.010 S: −0.120 ± 0.014	T: −0.133 ± 0.018 S: −0.223 ± 0.103	T: 115.4 (76–157.9)S: 69.77 (33.7–110.2)	T: 17.2 (16.8–17.7) *S: 16.3 (15.8–16.8)	T: 12.0 (11.4–12.7)S: 19.2 (17.1–21.8)	T: 12.3 (11.1–13.7)S: 15.9 (13.5–19.3)
	C	T: −0.010 ± 0.002 S: −0.012 ± 0.005	T: −0.011 ± 0.003 S: −0.005 ± 0.002	T: −0.046 ± 0.002 S: −0.016 ± 0.006	T: 4E-5 ± 0.001 S: 0.000 ± 0.001	T: 222.9 (183.7–263.3)S: 194.2 (104.5–292.5)	T: 218.1 (155.9–283.6) S: >192	T: 50.1 (47.2–53.3)S: 144.3 (97.0–248.8)	T: GrowthS: Growth
HL	*B*	T: −0.008 ± 0.01 S: −0.12 ± 0.00	T: −0.170 ± 0.012 S: −0.089 ± 0.015	T: −0.188 ± 0.019 S: −0.115 ± 0.017	T: −0.123 ± 0.08 S: −0.230 ± 0.079	T: 158.0 (136.2–180.2)* S: 18.7 (16.6–20.9)	T: 13.6 (12.6–14.7)S: 25.8 (21.1–30.6) *	T: 12.3 (11.1–13.7) S: 20.1 (17.2–23.9)	T: 18.7 (17.0–20.7) S: 10.0 (7.4–15.4)
	C	−0.005 ± 0.002	−0.082 ± 0.007	−0.097 ± 0.014	−9E-4 ± -8.8E-4	441.3 (215.3–686.0)	27.9 (25.5–30.8)	23.8 (20.6–28.2)	Growth
LL	*B*	T: −0.011 ± 0.00 S: −0.009 ± 0.00	T: −0.178 ± 0.009 S: −0.157 ± 0.009	T: −0.188 ± 0.020 S: −0.144 ± 0.024	T: −0.116 ± 0.09 S: −0.204 ± 0.122	T: 193.5 (115.2–278.5)S: 287.3 (169.9–332.6)*	T: 13.0 (12.3–13.7) S: 14.7 (13.8–15.6)	T: 12.3 (11.1–13.7)S: 15.9 (13.5–19.3)	T: 19.8 (18.2–21.7) S: 11.3 (7.0–28.3)
	C	−0.000 ± 0.002	−0.069 ± 0.013	−0.078 ± 0.017	−0.001 ± 0.009	3,021 (2,033 – 8,774)	33.3 (27.5–41.6)	29.4 (23.5–38.5)	Growth

*Higher than other treatments (pairwise comparison, Dunn test, $p < 0.05$). All values are reported as estimations (min–max). The minimum and maximum were calculated from the standard error of each model fit.

biomass could induce some shadowing that delayed viral RNA decay in the soluble fraction despite the oxidative effect of photo-oxygenation.

The affinity of each virus for solids and its capacity to survive after adsorption also influenced their overall survival. As a nonenveloped virus with less affinity for solids, MS2 showed relatively lower initial partitioning than the enveloped Phi6 and BCoV. However, MS2 increased its partitioning to solids over time, suggesting a proportionally slower decay in the solids than in the soluble fraction in all algal-bacterial photoreactors and *HLNP-C* (see Table 4). Similarly, BCoV partitioning to solids in all photobioreactors, including Phi6 in *LL-B,* remained high at least during the first 72 h, indicating a certain protective effect to photoinactivation and oxidation in the solids. In contrast, the decrease over time in solids partitioning of Phi6 in *HLNP-B* and *HL-B* and *uidA* in *HLNP-B* suggested a lower survival of the attached RNA. No direct associations between *uidA* partitioning to solids and reductions over time in *HL-B* and *LL-B* were detected, thus reinforcing the stronger influence of RNA decay in the soluble phase of the photobioreactors.

Regarding *uidA* gene, *E. coli* was added to the algal-bacterial and control photoreactors as a component of the Scourguard® vaccine and as cells that could pass 0.22 μm filtration of the MS2 stock solution achieved after amplification. The *uidA* gene marker was used as a proxy of *E. coli* decay rates in all algal-bacterial photoreactors. Previous works have reported similar *E. coli* inactivation of about 2.0 log_{10} units in sunlight and artificially illuminated photoreactors and high rate algal ponds due to high pH and reactive forms of oxygen (Young et al., 2016; Torres Franco et al., 2018; Silva et al., 2023), which were likely the predominating factors mediating inactivation in all algal-bacterial photoreactors. Similar to viral RNA, NPs in *HLNP-B* could enhance *uidA* reduction due to induced oxidative stress by producing reactive oxygen species (Lee et al., 2008). In all cases, a high reduction above 99 % demonstrated the potential of microalgae systems to eliminate viral RNA and *E. coli* fingerprint within typical HRTs of 2–8 days (e.g. Espinosa et al., 2021), providing treated effluents and biosolids of high sanitary quality and reducing further disinfection requirements.

4.2. Viral decays in abiotic control photoreactors

No significant increases in O_2 headspace concentrations, pH, or D.O changes were observed in the abiotic control photoreactors, which also showed lower MS2, Phi6 and *uidA* RNA reductions than the algal-bacterial photoreactors. Thus, the algal-bacterial activity was the main

Table 4
Viral RNA and *uidA* partitioning to solids in biodegradation (B) reactors at High light intensity + zero-valent iron nanoparticles (*HLNP*), High light intensity (*HL)*; and Low Light intensity (*LL*), including abiotic control (C) photoreactors in *HLNP*.

Gene	Time	Photoreactor			
		HLNP		*HL*	*LL*
		B	*C*	*B*	*B*
MS2	0	27 % ± 15	68 % ± 2	59 % ± 7	31 % ± 31
	24	49 % ± 0	52 % ± 6	97 % ± 0	5 % ± 5
	72	100 % ± 0	80 % ± 17	98 % ± 0	46 % ± 21
	192	99 % ± 0	70 % ± 0	95 % ± 5	45 % ± 14
Phi6	0	48 % ± 0	68 % ± 2	48 % ± 12	43 % ± 18
	24	54 % ± 18	43 % ± 0	15 % ± 15	41 % ± 18
	72	8 % ± 8	29 % ± 6	38 % ± 38	70 % ± 9
	192	2 % ± 2	31 % ± 31	15 % ± 15	0 % ± 0
BCoV	0	100 % ± 0	100 % ± 0	100 % ± 0	43 % ± 18
	24	98 % ± 1	50 % ± 50	99 % ± 1	41 % ± 18
	72	98 % ± 0	79 % ± 12	99 % ± 1	70 % ± 9
	192	0 % ± 0	82 % ± 15	0 % ± 0	0 % ± 0
uidA	0	0 % ± 0	50 % ± 5	0 % ± 0	0 % ± 0
	24	85 % ± 11	36 % ± 36	89 % ± 3	89 % ± 2
	72	23 % ± 23	41 % ± 8	21 % ± 3	0 % ± 2
	192	0 % ± 0	0 % ± 0	0 % ± 17	0 % ± 0

factor fostering the decay of these genes. Under abiotic conditions in *HLNP-C*, the high surface area of the ZVI NPs enhanced the hydrophobic interaction of all viral RNA and *uidA* gene, likely enhancing their partitioning to NPs, as also evidenced by the detection of fractions of RNA attached to agglomerated NPs retained in the 0.22 μm membranes (see Table 4). Indeed, detecting RNA associated with NPs in *HLNP-C* evidenced the formation of these agglomerates in *HLNP-C* and likely in *HLNP-B*. The attachment of RNA to NPs could mediate physical disruption or likely iron-related photocatalytic mechanisms (Pecson et al., 2012), contributing to the decay of MS2 and BCoV, which showed a higher partitioning to ZVI NPs in *HLNP-C*. However, the influence of these mechanisms was limited since reductions lower than 90 % were found for MS2, Phi6 and *uidA* in *HLNP-C*, probably due to the neutral pH and anoxic conditions preventing iron oxidation and further formation of reactive species.

In the case of BCoV, the rapid decay and high $\log_{10}$ units removed in all abiotic controls suggest that its RNA was proportionally more damaged by a light-driven mechanism than by photo-oxygenation in the presence or absence of ZVI NPs. The lower reductions of Phi6 and MS2 than that of BCoV in the abiotic controls suggest a proportionally less intense effect of light-driven mechanisms and only a marginal effect for the MS2 bacteriophage. Furthermore, the higher decay rates of Phi6 and BCoV in *HL-C* and *LL-C* also suggest that ZVI NPs could exhibit a shadowing effect that eventually enhanced the survival of these viruses.

Conversely, the higher $\log_{10}$ units reduction recorded for MS2 compared to those for the other target genes in the presence of ZVI NPs (in both biodegradation and abiotic assays) can be related to the lack of a positively charged structural part in this bacteriophage, enhancing the negative effect of oxidised ZVI (Raza et al., 2022). Overall, an intrinsic contribution of ZVI NPs seemed to be relevant mainly in the inactivation of MS2, while the higher reductions achieved in *HLNP-B* for all target genes were likely mediated by the enhancement of photo-oxygenation in the presence of ZVI NPs and light exposure, mainly for Phi6 and MS2.

On the other hand, by comparing decay parameters with previous works in water matrixes, a higher persistence of MS2, Phi6, BCoV and *uidA* RNA than expected for infective particles was observed. For instance, previous reports suggested a faster decay of infective MS2 in pasteurised wastewater (T_{90} of 121 h at 25 °C, Ye et al., 2016), sterilised river water (187 h, 20 °C, Sala-Comorera et al., 2021), or experiments at a similar illumination and same abiotic *SMWW* (T_{90} of 32 h, Torres-Franco et al., 2024). Indeed, at a similar light intensity of *HL-B* and the same *SMWW* composition, infective Phi6 showed a T_{90} of 11 h (Torres-Franco et al., 2024), lower than the period of about 30 h herein reported. Despite the fact that few experiments assessed its survival in wastewater matrixes, BCoV RNA was detected following 55 days of the spike in wastewater and was not detected under anaerobic conditions after 120 h (Guérin-Rechdaoui et al., 2022), also showing a relatively high persistence of its fingerprint in wastewater environments. When comparing BCoV and SARS-CoV-2 RNA, T_{90} values of infective particles and RNA were reported in 40 h (Bivins et al., 2020) and 36 h (de Oliveira et al., 2021), also higher than T_{90} of 23.8 h and 29.4 h herein detected for BCoV RNA in *LL-C* and *HL-C*, respectively.

This trend to a higher persistence of RNA fingerprint compared to infective particles in water matrixes was also suggested in previous works. For MS2, Sala-Comorera et al. (2021) detected no decay of RNA signal in river water after 480 h (20 days) when infectious particles showed T_{90} of 187 h. Similarly, MS2 RNA showed no decay during co-incubation in a salt medium with *N. salina* after 312 h, whereas infective particles were reduced to non-detectable after 8 h (Unnithan et al., 2014). Moreover, for Phi6 decay in carpet and dust, T_{90} for RNA was at least ten-fold the values for infective particles (Nastasi et al., 2022).

Regarding *uidA* gene, a higher bactericidal effect of ZVI NPs on *E. coli* under anaerobic compared to aerobic conditions was previously suggested by Lee et al. (2008) due to the higher nanoparticle dosage that may be required due to corrosion. The removal of about 62 % of *uidA* gene after 192 in *HL-C* suggests that prolonged exposure time and light availability could improve *E. coli* inactivation at the low ZVI NPs dosage of 20 mg L^{-1} compared with an Ec_{50} of about 1 g L^{-1} in water media previously quantified for *E. coli* after 3 h exposure (Semerád et al., 2018). However, the reductions and decay of *uidA* herein achieved were considerably lower in all abiotic controls than in the aerobic conditions of the biodegradation photoreactors, indicating that microalgal-bacterial photo-oxygenation was the main factor mediating *uidA* reduction, with a further enhancement achieved by ZVI NPs addition. Finally, the increases in *uidA* genes in *HL-C* and *LL-C* could also be related to the extended survival of this genetic marker reported in polluted water matrixes (Brooks et al., 2015), reinforcing the evidence of a negative effect of ZVI NPs on *E. coli* during photo-oxygenation, but suggesting no harmful effect on water microbiota at the low dosage of ZVI NPs and in the absence of intense microalgal-bacterial activity.

4.3. Challenges in NPs-based disinfection in microalgae systems

In full-scale implementations, magnetic separation of microalgae biomass and NPs, and regeneration using a low concentration of alkali combined with ultrasonication, is a promising technology that exhibits no limitations for further valorisation of microalgae biomass through anaerobic digestion (Markeb et al., 2019). These steps could be integrated into sewage treatment via anaerobic digestion coupled with algal ponds, a technology with a positive energy balance (Vassalle et al., 2020). Nonetheless, direct fertigation with the microalgae-NPs may save separation costs and take advantage of a possible synergistic effect of microalgae fertiliser or biostimulant properties (Álvarez-González et al., 2022) and ZVI NPs. Indeed, these NPs were previously identified as seed priming agents without any toxic effect on plants at concentrations of <80 mg L^{-1} (Guha et al., 2018) and minor intrinsic NPs toxicity effect on soil and water microbiota compared to E_{50} values of 0.3–1.1 g L^{-1} (Semerád et al., 2018). In addition, the use of liquid NPs solutions, which do not require prior drying and entail similar effects in terms of enhancement of photosynthetic activity, will significantly reduce the cost of NPs addition to any biotechnological process (Hoyos et al., 2024). Further studies should assess the cost-effectiveness and regulatory compliance of different scenarios of biomass and effluent downstream applications and ZVI NPs accumulation on receiving soil or water bodies.

5. Conclusions

Algal-bacterial photoreactors operated at high and low light intensity resulted in at least 99.9 % reductions in the bulk fraction of viral RNA from MS2, Phi6 and BCoV, and 99 % of *uidA* gene from *E. coli* within 192 h. The addition of a low dosage of ZVI NPs (20 mg L^{-1}) at high light intensity enhanced within 96 h the TN and TOC removals and provided at least 90 % reductions within 72 h of all target genes, supporting a similar performance to that achieved within 192 h in the absence of nanoparticles. For the first time, the potential of ZVI NPs to enhance virus and *E. coli* reductions during secondary microalgal-based wastewater treatment was demonstrated.

CRediT authorship contribution statement

Andrés F. Torres-Franco: Conceptualization, Data curation, Investigation, Methodology, Writing – original draft, Writing – review & editing. **Deborah Leroy-Freitas:** Writing – review & editing, Writing – original draft, Methodology, Investigation. **Pedro A. García-Encina:** Writing – review & editing, Writing – original draft, Resources, Project administration, Methodology, Conceptualization. **Raúl Muñoz:** Writing – review & editing, Writing – original draft, Supervision, Resources, Methodology, Conceptualization.

Declaration of competing interest

The authors declare that they have no known competing financial interests or personal relationships that could have appeared to influence the work reported in this paper.

Acknowledgements

This work was performed with financial support from the Regional Government of Castilla y León and the FEDER program (projects CLU 2017-09, CL-EI-2021-07, UIC315, and VA266P20). Araceli Crespo and Enrique Marcos are acknowledged for their technical assistance in solids and TOC analyses.

Appendix A. Supplementary data

Supplementary data to this article can be found online at https://doi.org/10.1016/j.biortech.2025.132389.

Data availability

Data will be made available on request.

References

Álvarez-González, A., Uggetti, E., Serrano, L., Gorchs, G., Ferrer, I., Díez-Montero, R., 2022. Can microalgae grown in wastewater reduce the use of inorganic fertilizers? Journal of environmental management 323, 116224.

Bivins, A., Greaves, J., Fischer, R., Yinda, K.C., Ahmed, W., Kitajima, M., Munster, V.J., Bibby, K., 2020. Persistence of SARS-CoV-2 in water and wastewater. Environ. Sci. Technol. Lett. 7 (12), 937–942. https://doi.org/10.1021/acs.estlett.0c00730.

Brooks, Y., Aslan, A., Tamrakar, S., Murali, B., Mitchell, J., Rose, J.B., 2015. Analysis of the persistence of enteric markers in sewage polluted water on a solid matrix and in liquid suspension. Water Res. 76, 201–212. https://doi.org/10.1016/j.watres.2015.02.039.

Chern, E.C., Brenner, K.P., Wymer, L., Haugland, R.A., 2009. Comparison of fecal indicator bacteria densities in marine recreational waters by QPCR. Water Expo. Health 1, 203–214. https://doi.org/10.1007/s12403-009-0019-2.

Coudray-Meunier, C., Fraisse, A., Martin-Latil, S., Delannoy, S., Fach, P., Perelle, S., 2016. A novel high-throughput method for molecular detection of human pathogenic viruses using a nanofluidic real-time PCR system. PLoS One 11 (1), e0147832. https://doi.org/10.1371/journal.pone.0147832.

De Oliveira, L.C., Torres-Franco, A.F., Lopes, B.C., da Silva Santos, B.S., Costa, E.A., Costa, M.S., Reis, M.T., Melo, M.C., Polizzi, R.B., Teixeira, M.M., Mota, C.R., 2021. Viability of SARS-CoV-2 in river water and wastewater at different temperatures and solids content. Water Res. 195, 117002. https://doi.org/10.1016/j.watres.2021.117002.

Decaro, N., Elia, G., Campolo, M., Desario, C., Mari, V., Radogna, A., Buonavoglia, C., 2008. Detection of bovine coronavirus using a TaqMan-based real-time RT-PCR assay. J. Virol. Methods 151 (2), 167–171. https://doi.org/10.1016/j.jcis.2014.08.055.

Decrey, L., Kazama, S., Udert, K.M., Kohn, T., 2015. Ammonia as an in situ sanitizer: inactivation kinetics and mechanisms of the ssRNA virus MS2 by NH3. Environ. Sci. Technol. 49 (2), 1060–1067.

Delanka-Pedige, H.M., Cheng, X., Munasinghe-Arachchige, S.P., Abeysiriwardana-Arachchige, I.S., Xu, J., Nirmalakhandan, N., Zhang, Y., 2020. Metagenomic insights into virus removal performance of an algal-based wastewater treatment system utilizing Galdieria sulphuraria. Algal Research 47, 101865.

Dika, C., Duval, J.F., Francius, G., Perrin, A., Gantzer, C., 2015. Isoelectric point is an inadequate descriptor of MS2, Phi X 174 and PRD1 phages adhesion on abiotic surfaces. J. Colloid Interface Sci. 446, 327–334. https://doi.org/10.1016/j.jcis.2014.08.055.

Espinosa, M.F., Verbyla, M.E., Vassalle, L., Rosa-Machado, A.T., Zhao, F., Gaunin, A., Mota, C.R., 2021. Reduction and partitioning of viral and bacterial indicators in a UASB reactor followed by high rate algal ponds treating domestic sewage. Sci. Total Environ. 760, 144309. https://doi.org/10.1016/j.scitotenv.2020.144309.

Fedorenko, A., Grinberg, M., Orevi, T., Kashtan, N., 2020. Survival of the enveloped bacteriophage Phi6 (a surrogate for SARS-CoV-2) in evaporated saliva microdroplets deposited on glass surfaces. Sci. Rep. 10 (1), 1–10. https://doi.org/10.1038/s41598-020-79625-z.

Frutos, O.D., Quijano, G., Perez, R., Munoz, R., 2016. Simultaneous biological nitrous oxide abatement and wastewater treatment in a denitrifying off-gas bioscrubber. Chem. Eng. J. 288, 28–37. https://doi.org/10.1016/j.cej.2015.11.088.

García, A., Le, T., Jankowski, P., Yanaç, K., Yuan, Q., Uyaguari-Diaz, M.I., 2022. Quantification of human enteric viruses as alternative indicators of fecal pollution to evaluate wastewater treatment processes. PeerJ 10, e12957. https://doi.org/10.7717/peerj.12957.

Gonzalez-Camejo, J., Viruela, A., Ruano, M.V., Barat, R., Seco, A., Ferrer, J., 2019. Effect of light intensity, light duration and photoperiods in the performance of an outdoor photobioreactor for urban wastewater treatment. Algal Res. 40, 101511. https://doi.org/10.1016/j.algal.2019.101511.

Greenwald, H., Kennedy, L.C., Kantor, K.L.N. 2021. One-Step RT-qPCR for SARS-CoV-2 Wastewater Surveillance: N1, PMMoV, BCoV, SOC, CrAssphage, Bacteroides rRNA, 18S rRNA. protocols.io. https://dx.doi.org/10.17504/protocols.io.bsgvnbw6.

Guérin-Rechdaoui, S., Bize, A., Levesque-Ninio, C., Janvier, A., Lacroix, C., Le Brizoual, F., Rocher, V., 2022. Fate of SARS-CoV-2 coronavirus in wastewater treatment sludge during storage and thermophilic anaerobic digestion. Environ. Res. 214, 114057. https://doi.org/10.1016/j.envres.2022.114057.

Guha, T., Ravikumar, K.V.G., Mukherjee, A., Mukherjee, A., Kundu, R., 2018. Nanopriming with zero valent iron (nZVI) enhances germination and growth in aromatic rice cultivar (Oryza sativa cv. Gobindabhog L.). Plant Physiol. Biochem. 127, 403–413. https://doi.org/10.1016/j.plaphy.2018.04.014.

Gutierrez, L., Li, X., Wang, J., Nangmenyi, G., Economy, J., Kuhlenschmidt, T.B., Nguyen, T.H., 2009. Adsorption of rotavirus and bacteriophage MS2 using glass fiber coated with hematite nanoparticles. Water Res. 43 (20), 5198–5208. https://doi.org/10.1016/j.watres.2009.08.031.

Harrison, K.R., Snead, D., Kilts, A., Ammerman, M.L., Wigginton, K.R., 2023. The protective effect of virus capsids on RNA and DNA virus genomes in wastewater. Environ. Sci. Technol. 57 (37), 13757–13766. https://doi.org/10.1021/acs.est.3c03814.

Hoyos, E.G., Kuri, R., Toda, T., Muñoz, R., 2024. Innovative design and operational strategies to improve CO_2 mass transfer during photosynthetic biogas upgrading. *Bioresour. Technol.* 391, 129955. https://doi.org/10.1016/j.biortech.2023.129955.

Jafferali, M.H., Khatami, K., Atasoy, M., Birgersson, M., Williams, C., Cetecioglu, Z., 2021. Benchmarking virus concentration methods for quantification of SARS-CoV-2 in raw wastewater. Sci. Total. Environ. 755, 142939. https://doi.org/10.1016/j.scitotenv.2020.142939.

Kapil, S., Richardson, K.L., Maag, T.R., Goyal, S.M., 1999. Characterization of bovine coronavirus isolates/from eight different states in the USA. Vet. Microbiol. 67 (3), 221–230. https://doi.org/10.1016/S0378-1135(99)00042-5.

Kennedy, L.C., Costantini, V.P., Huynh, K.A., Loeb, S.K., Jennings, W.C., Lowry, S., Boehm, A.B., 2023. Persistence of human norovirus (GII) in surface water: decay rate constants and inactivation mechanisms. Environ. Sci. Technol. 57 (9), 3671–3679. https://doi.org/10.1021/acs.est.2c09637.

Kim, J.Y., Lee, C., Love, D.C., Sedlak, D.L., Yoon, J., Nelson, K.L., 2011. Inactivation of MS2 coliphage by ferrous ion and zero-valent iron nanoparticles. Environ. Sci. Technol. 45 (16), 6978–6984. https://doi.org/10.1021/es201345y.

Kim, K., Jothikumar, N., Sen, A., Murphy, J.L., Chellam, S., 2021. Removal and inactivation of an enveloped virus surrogate by iron conventional coagulation and electrocoagulation. Environ. Sci. Technol. 55 (4), 2674–2683. https://doi.org/10.1021/acs.est.0c07697.

Kingsley, D.H., Fay, J.P., Calci, K., Pouillot, R., Woods, J., Chen, H., Van Doren, J.M., 2017. Evaluation of chlorine treatment levels for inactivation of human norovirus and MS2 bacteriophage during sewage treatment. Appl. Environ. Microbiol. 83 (23), e01270–e01317. https://doi.org/10.1128/AEM.01270-17.

Nastasi, N., Renninger, N., Bope, A., Cochran, S.J., Greaves, J., Haines, S.R., Dannemiller, K.C., 2022. Persistence of viable MS2 and Phi6 bacteriophages on carpet and dust. Indoor Air 32 (1), e12969. https://doi.org/10.1111/ina.12969.

Lee, C., Kim, J.Y., Lee, W.I., Nelson, K.L., Yoon, J., Sedlak, D.L., 2008. Bactericidal effect of zero-valent iron nanoparticles on Escherichia coli. Environ. Sci. Technol. 42 (13), 4927–4933. https://doi.org/10.1021/es800408u.

McCall, C., Wu, H., Miyani, B., Xagoraraki, I., 2020. Identification of multiple potential viral diseases in a large urban center using wastewater surveillance. Water Res. 184, 116160. https://doi.org/10.1016/j.watres.2020.116160.

Markeb, A.A., Llimós-Turet, J., Ferrer, I., Blánquez, P., Alonso, A., Sánchez, A., Font, X., 2019. The use of magnetic iron oxide based nanoparticles to improve microalgae harvesting in real wastewater. Water Res. 159, 490–500. https://doi.org/10.1016/j.watres.2019.05.023.

Miranda, J.A., Steward, G.F., 2017. Variables influencing the efficiency and interpretation of reverse transcription quantitative PCR (RT-qPCR): An empirical study using Bacteriophage MS2. J. Virol. Methods 241, 1–10. https://doi.org/10.1016/j.jviromet.2016.12.002.

Nieto-Juarez, J.I., Kohn, T., 2013. Virus removal and inactivation by iron (hydr) oxide-mediated Fenton-like processes under sunlight and in the dark. Photochem. Photobiol. Sci. 12 (9), 1596–1605. https://doi.org/10.1039/c3 pp25314g.

Onofri, A. (2020). Aomisc: Statistical methods for the agricultural sciences. R package version 0.62.

Pecson, B.M., Decrey, L., Kohn, T., 2012. Photoinactivation of virus on iron-oxide coated sand: enhancing inactivation in sunlit waters. Water Res. 46 (6), 1763–1770. https://doi.org/10.1016/j.watres.2011.12.059.

Posadas, E., del Mar Morales, M., Gomez, C., Acién, F.G., Muñoz, R., 2015. Influence of pH and CO_2 source on the performance of microalgae-based secondary domestic wastewater treatment in outdoors pilot raceways. Chem. Eng. J. 265, 239–248. https://doi.org/10.1016/j.cej.2014.12.059.

Prado, T., Bruni, A.D.C., Barbosa, M.R.F., Sato, M.I.Z., 2018. Distribution of human fecal marker GB-124 bacteriophages in urban sewage and reclaimed water of São Paulo city, Brazil. J. Water Health 16 (2), 289–299. https://doi.org/10.2166/wh.2017.011.

Randazzo, W., Truchado, P., Cuevas-Ferrando, E., Simón, P., Allende, A., Sánchez, G., 2020. SARS-CoV-2 RNA in wastewater anticipated COVID-19 occurrence in a low prevalence area. Water Res. 181, 115942. https://doi.org/10.1016/j.watres.2020.115942.

Raza, S., Folga, M., Łoś, M., Foltynowicz, Z., Paczesny, J., 2022. The effect of zero-valent iron nanoparticles (nZVI) on bacteriophages. Viruses 14 (5), 867. https://doi.org/10.3390/v14050867.

Rice, E.W., Bridgewater, L., American Public Health Association (Eds.)., 2012. Standard methods for the examination of water and wastewater (Vol. 10). Washington, DC: American public health association.

Ritz, C., Baty, F., Streibig, J.C., Gerhard, D., 2015. Dose-response analysis using R. PLoS One 10 (12), e0146021.

Ruas, G., Farias, S.L., Scarcelli, P.G., Serejo, M.L., Boncz, M.A., 2020. The effect of CO_2 addition and hydraulic retention time on pathogens removal in HRAPs. Water Sci. Technol. 82 (6), 1184–1192. https://doi.org/10.2166/wst.2020.255.

Sala-Comorera, L., Reynolds, L.J., Martin, N.A., O'Sullivan, J.J., Meijer, W.G., Fletcher, N.F., 2021. Decay of infectious SARS-CoV-2 and surrogates in aquatic environments. Water Res. 201, 117090. https://doi.org/10.1016/j.watres.2021.117090.

Semerád, J., Čvančarová, M., Filip, J., Kašlík, J., Zlotá, J., Soukupová, J., Cajthaml, T., 2018. Novel assay for the toxicity evaluation of nanoscale zero-valent iron and derived nanomaterials based on lipid peroxidation in bacterial species. Chemosphere 213, 568–577. https://doi.org/10.1016/j.chemosphere.2018.09.029.

Silva, L.M.L., Santiago, F.A., Da Silva, G.A., De Lima, L.B., Amaral, L.P., Nascimento, R.S. L., 2023. Inactivation of Escherichia coli in photobioreactors with microalgae and illuminated by light emitting diodes. Int. J. Environ. Sci. Technol. 20 (1), 63–74. https://doi.org/10.1007/s13762-022-03990-7.

Silverman, A.I., Boehm, A.B., 2020. Systematic review and meta-analysis of the persistence and disinfection of human coronaviruses and their viral surrogates in water and wastewater. Environ. Sci. Technol. Lett. 7 (8), 544–553. https://doi.org/10.1021/acs.estlett.0c00313.

Torres Franco, A.F., da Encarnação Araújo, S., Passos, F., de Lemos Chernicharo, C.A., Mota Filho, C.R., Cunha Figueredo, C., 2018. Treatment of food waste digestate using microalgae-based systems with low-intensity light-emitting diodes. Water Sci. Technol. 78 (1), 225–234. https://doi.org/10.2166/wst.2018.198.

Torres-Franco, A.F., Leroy-Freitas, D., Martinez-Fraile, C., Rodríguez, E., García-Encina, P.A., Muñoz, R., 2024. Partitioning and inactivation of enveloped and nonenveloped viruses in activated sludge, anaerobic and microalgae-based wastewater treatment systems. Water Res. 248, 120834. https://doi.org/10.1016/j.watres.2023.120834.

Titcombe Lee, M., Pruden, A., Marr, L.C., 2016. Partitioning of viruses in wastewater systems and potential for aerosolization. Environ. Sci. Technol. Lett. 3 (5), 210–215. https://doi.org/10.1021/acs.estlett.6b00105.

Vargas-Estrada, L., Torres-Arellano, S., Longoria, A., Arias, D.M., Okoye, P.U., Sebastian, P.J., 2020. Role of nanoparticles on microalgal cultivation: a review. Fuel 280, 118598. https://doi.org/10.1016/j.fuel.2020.118598.

Unnithan, V.V., Unc, A., Smith, G.B., 2014. Role of Nannochloropsis salina for the recovery and persistence of MS2 virus in wastewater. Algal Research 4, 70–75.

Vargas-Estrada, L., Hoyos, E.G., Sebastian, P.J., Muñoz, R., 2023. Influence of mesoporous iron based nanoparticles on Chlorella sorokiniana metabolism during photosynthetic biogas upgrading. Fuel 333, 126362. https://doi.org/10.1016/j.fuel.2022.126362.

Vassalle, L., Díez-Montero, R., Machado, A.T.R., Moreira, C., Ferrer, I., Mota, C.R., Passos, F., 2020. Upflow anaerobic sludge blanket in microalgae-based sewage treatment: co-digestion for improving biogas production. Bioresour. Technol. 300, 122677. https://doi.org/10.1016/j.biortech.2019.122677.

Verbyla, M.E., Symonds, E.M., Kafle, R.C., Cairns, M.R., Iriarte, M., Mercado Guzman, A., Mihelcic, J.R., 2016. Managing microbial risks from indirect wastewater reuse for irrigation in urbanizing watersheds. Environ. Sci. Technol. 50 (13), 6803–6813. https://doi.org/10.1021/acs.est.5b05398.

Vlasova, A.N., Saif, L.J., 2021. Bovine coronavirus and the associated diseases. Front. Vet. Sci. 8, 643220. https://doi.org/10.3389/fvets.2021.643220.

Wang, J., Liu, C., Sun, H., Wang, S., Liao, X., Zhang, L., 2022. Membrane disruption boosts iron overload and endogenous oxidative stress to inactivate Escherichia coli by nanoscale zero-valent iron. J. Hazard. Mater. 435, 128951. https://doi.org/10.1016/j.jhazmat.2022.128951.

Wang, Y.Y., Cheng, H.X., Zheng, L.Y., Luo, L.Z., Liu, J.Z., Zhang, M., Tian, G.M., 2024. Synergistic promotion of microalgal growth and copper removal from synthetic wastewater by nanoscale zero-valent iron particles. Environ. Technol. 1–13. https://doi.org/10.1080/09593330.2024.2354055.

Yang, W., Cai, C., Dai, X., 2022. Interactions between virus surrogates and sewage sludge vary by viral analyte: recovery, persistence, and sorption. Water Res. 210, 117995. https://doi.org/10.1016/j.watres.2021.117995.

Ye, Y., Ellenberg, R.M., Graham, K.E., Wigginton, K.R., 2016. Survivability, partitioning, and recovery of enveloped viruses in untreated municipal wastewater. Environ. Sci. Technol. 50 (10), 5077–5085. https://doi.org/10.1021/acs.est.6b00876.

Young, P., Buchanan, N., Fallowfield, H.J., 2016. Inactivation of indicator organisms in wastewater treated by a high rate algal pond system. J. Appl. Microbiol. 121 (2), 577–586. https://doi.org/10.1111/jam.13180. PMID: 27187055.